Chinese Chemical Letters 37 (2026) 111353

Contents lists available at ScienceDirect

Chinese Chemical Letters

journal homepage: www.elsevier.com/locate/cclet

Self-assembly of disassemblable supramolecular organic frameworks for doxorubicin delivery, photofrin posttreatment phototoxicity inhibition and heparin neutralization

Ya-Jie Zhu[a], Zhi-Min Lv[a], Hao-Feng Zhu[a], Qi-Yan Qi[a], Shang-Bo Yu[a,*], Jia Tian[a], Wei Zhou[b,*], Zhan-Ting Li[a,*]

[a] State Key Laboratory of Organometallic Chemistry, Shanghai Institute of Organic Chemistry, Chinese Academy of Sciences, University of Chinese Academy of Sciences, Shanghai 200032, China
[b] Department of Chemistry, Fudan University, Shanghai 200438, China

ARTICLE INFO

Article history:
Received 14 March 2025
Revised 8 May 2025
Accepted 19 May 2025
Available online 20 May 2025

Keywords:
Supramolecular organic framework
Self-assembly and disassembly
Biosafety
Drug delivery
Porphyrin phototoxicity inhibition
Heparin antagonism

ABSTRACT

Two supramolecular organic frameworks (SOFs) have been constructed from the co-assembly of biimidazolium-derived octacationic components and cucurbit[8]uril in water. Dynamic light scattering and ^{1}H NMR experiments reveal that both SOFs can undergo reversible assembly and disassembly at room temperature. One of the SOFs displays unprecedently high maximum tolerated dose of 120 mg/kg with mice, which improves by 40% compared with the highest value of the reported SOFs. *In vitro* and *in vivo* tests show that the SOF can adsorb doxorubicin and overcome the resistance of multidrug-resistant MDR A549/ADR tumor cells to realize intracellular delivery, leading to enhanced antitumor efficacy. Moreover, it can also completely inhibit the posttreatment phototoxicity of photofrin and fully neutralize the anticoagulation of both unfractionated heparin and low molecular weight heparins through efficient inclusion and elimination or sequestration mechanism. As the first examples that undergo room-temperature reversible assembly and disassembly, the new SOFs in principle allow for quantitative analysis of the molecular components in the body that is prerequisite for preclinical evaluation in the future.
© 2025 Published by Elsevier B.V. on behalf of Chinese Chemical Society and Institute of Materia Medica, Chinese Academy of Medical Sciences.

Self-assembly features reversibility due to the dynamics of non-covalent forces, which endows the fabrication and decomposition of supramolecular architectures with stimulus-responsive regulation [1–3]. By making use of this character, chemists have developed a variety of delivering systems that exhibit stimuli-responsive drug release and efficacy enhancement [4–14]. Since the microenvironment of many tumors is typically weakly acidic [15], hypoxic [16,17] and spermine-rich [18–21], in recent years chemists also have considerable interest in developing supramolecular delivering systems which are responsive to these features. Despite these important advances, the majority of clinical applications are related with liposomal drug delivery systems [22,23], although other systems such as albumin-bound and polymer micelle-formulated paclitaxel have also been approved for clinical use [24,25]. Given the complexity of formulation, low stability and high cost of liposomal drugs [26], the development of new kinds of delivery systems that overcome these drawbacks is highly demanded.

In the past decades, chemists have a considerable interest in developing bioactive molecules and supramolecular systems *via* cucurbit[*n*]uril-based host-guest complexation [27–39]. Among others, cucurbit[8]uril features the 1:2 binding pattern by including two aromatic guests [40–44]. In 2014, we reported the construction of the first three-dimensional (3D) water-soluble supramolecular organic framework (SOF) by hydrophobically driven co-assembly of a tetrahedral compound and cucurbit[8]uril (CB[8]) [45]. Such SOFs have inherent, regular pores of >2 nm apertures and can *in situ* include drugs and DNA to achieve intracellular delivery or activity suppression [46–52]. In particular, they display important nanoparticle effect to overcome the resistance of multidrug resistant human breast MCF-7/Adr cancer cells, leading to important enhancement of antitumor efficacy [46,47]. Nevertheless, all the 3D SOFs are generated at high concentrations of the components in boiling water and their disassembly upon dilution at room temperature occurs very slowly [45,51], which does not allow for quantitative analysis *in vitro* and *in vivo* and thus significantly reduce their potential for preclinical evaluation due to challenges for their absorption, metabolism, distribution and excretion of drugs in the body. Moreover, the highest maximum tol-

* Corresponding authors.
E-mail addresses: yushbo@sioc.ac.cn (S.-B. Yu), zhouw@fudan.edu.cn (W. Zhou), ztli@mail.sioc.ac.cn (Z.-T. Li).

https://doi.org/10.1016/j.cclet.2025.111353
1001-8417/© 2025 Published by Elsevier B.V. on behalf of Chinese Chemical Society and Institute of Materia Medica, Chinese Academy of Medical Sciences.

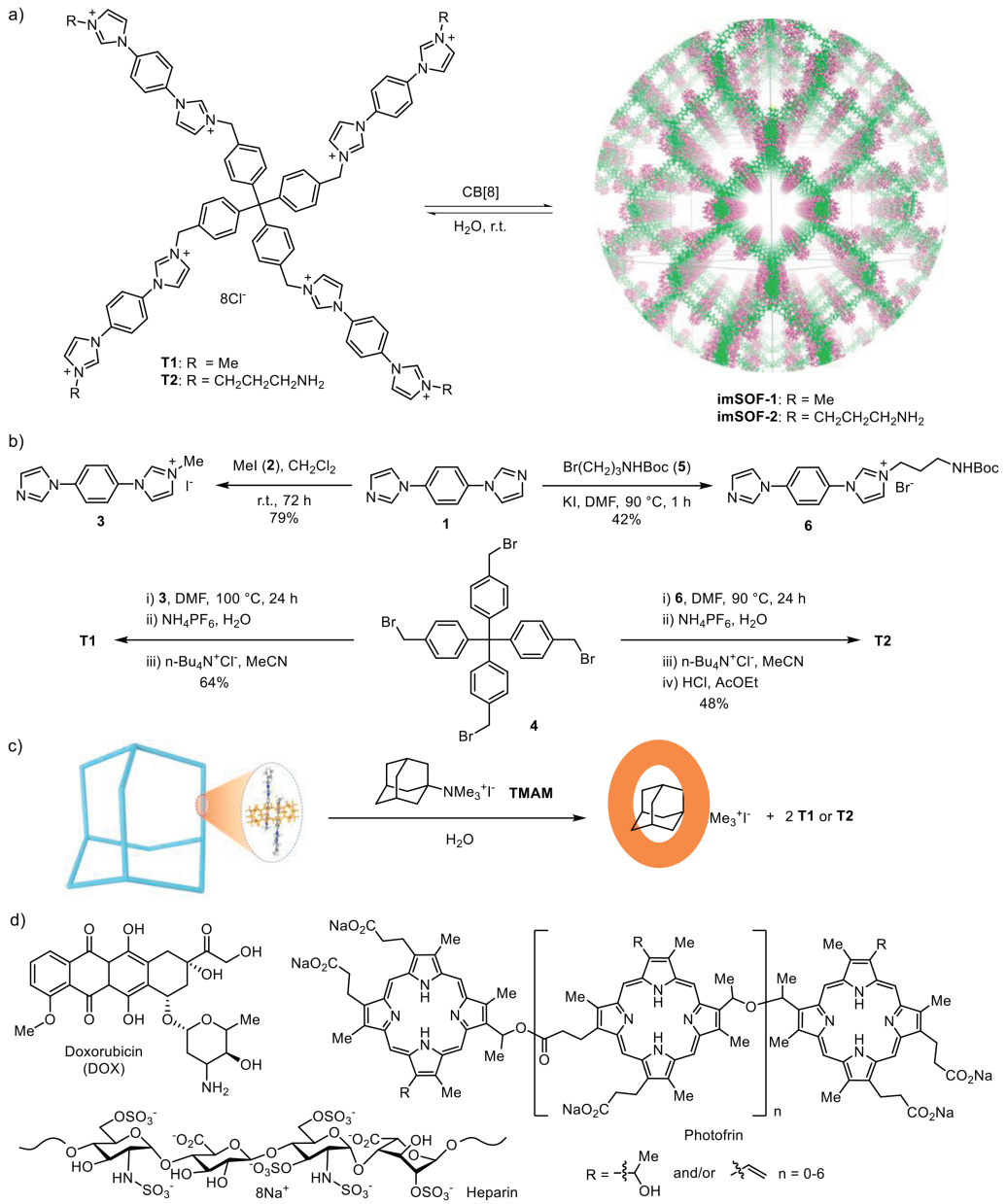


Fig. 1. (a) Assembly of **imSOF-1** and **imSOF-2** from **T1** or **T2** and CB[8]. (b) Preparation of **T1** and **T2**. (c) Substitution of TMAM for biimidazolium dimer in CB[8] leading to the decomposition of SOFs. (d) The structure of doxorubicin, photofrin, a heparin repeat unit.

erated dose with mice reported for 3D SOFs is 85 mg/kg [52]. Given that delivery systems are typically substantially excessive compared with delivered drugs [53,54], further improvement of the biosafety is highly demanded for possible preclinic evaluation. Here we report that, for the first time, 3D SOFs can be formed and decomposed at room temperature. We further demonstrate that the new SOFs display much improved biosafety and can include doxorubicin for intracellular delivery and antitumor activity enhancement and heparins as well as photofrin for inhibiting their anticoagulation or posttreatment phototoxicity.

CB[8] has the unique ability of including two hydrophobic aromatic units to form ternary complexes [41,55]. Tetrahedral precursors have been demonstrated to be ideal for constructing 3D porous frameworks with the structural feature of diamond [56]. In search for new tetrahedral components, we prepared compounds **T1** and **T2** to co-assemble with CB[8] to construct supramolecular organic frameworks **imSOF-1** and **imSOF-2** (Fig. 1a). Their synthetic routes are shown in Fig. 1b. Briefly, compound **1** [57] was reacted with methyl iodide (**2**) to afford compound **3** in 79% yield. The intermediate was then treated with **4** [58] to give **T1** in 64% yield after ion exchange. For the preparation of **T2**, **1** was first treated with **5** to produce **6** in 42% yield. The latter was further reacted with **3** to afford **T2** in 48% yield after ion exchange and removal of the Boc protection group with hydrochloride. Both **T1** and **T2** are highly soluble in water (>300 mmol/L).

Adding 0.5 equiv. of **T1** or **T2** to the suspended solution of CB[8] (600 mmol/L) in water caused CB[8] to dissolve quickly to give rise to a transparent solution, indicating that the resulting supramolecular organic frameworks **imSOF-1** and **imSOF-2** had at least solubility of 300 mmol/L, as represented by the concentration of the tetrahedral component. To get insight into the structure of the frameworks, ^{1}H NMR titration experiments were conducted by adding CB[8] to the solution of **T1** or **T2** (5 mmol/L) in D_2O (Figs. S1 and S2 in Supporting information). In both cases,

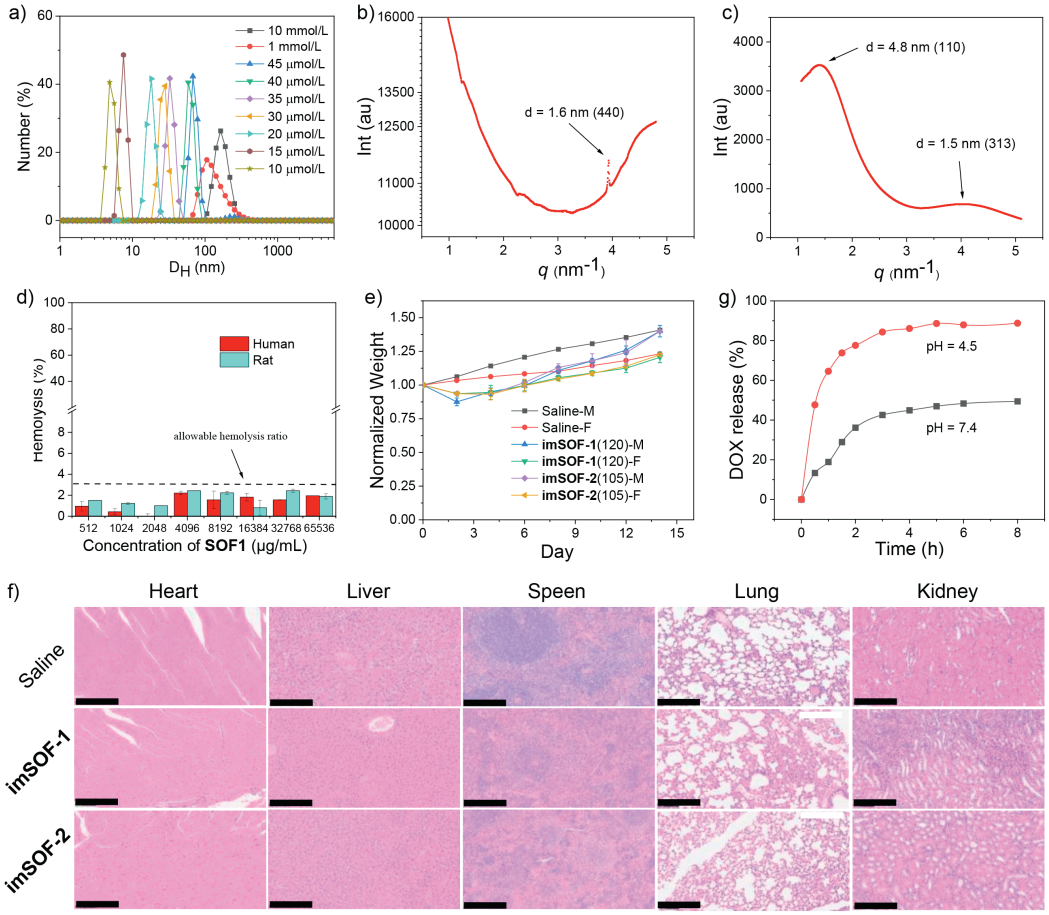


Fig. 2. (a) DLS profile of **imSOF-1** in water. (b) solid-state synchrotron SAXS profile of **imSOF-1**. (c) Solution-phase synchrotron SAXS profile of im**SOF-1** ([**T1**] = 0.2 mol/L) in water. (d) Hemolytic activity of **imSOF-1** with SD rat and human erythrocytes. Data are presented as mean ± SEM (n = 3). (e) Body weight of mice after intravenous injection of **imSOF-1** and **imSOF-2** of MTD (n = 6, 3 female + 3 male). (f) Representative pathological morphology of main organs of male mice harvested after euthanasia on day 14 after administration of saline, **imSOF-1** (120 mg/kg) and **imSOF-2** (105 mg/kg). Tissues were stained with hematoxylin and eosin and observed under a light microscope. (f) Representative pathological morphology of main organs harvested after euthanasia on day 14 after administration of saline (male) and **imSOF-1** (120 mg/kg, male) and **imSOF-2** (105 mg/kg, male). Tissues were stained with hematoxylin and eosin and observed under a light microscope (scale bar: 200 μm). (g) Dialysis profile for the release of DOX (0.1 mmol/L) from dialysis bag (1.5 mL, cutoff MW: 1000) to outside water (15 mL) at 37 °C against time in the presence and absence of **imSOF-1** ([**T1**] = 0.1 mmol/L) in the bag. The solutions were prepared in PBS (pH 7.4) buffer and AcOH/AcONa buffer (pH 4.5).

adding 2 equiv. of CB[8] caused the signals of the aromatic protons to disappear, which was accompanied with the formation of new broad signals of low resolution. This result supported that the hydrophobic aromatic arms of **T1** and **T2** was encapsulated with CB[8] through a 2:1 binding pattern, as established for 4-phenylpyridinium-derived SOFs [51]. Adding CB[8] to the aqueous solution of **T1** or **T2** (10 μmol/L) also caused continual hypochromic effect of their absorbance around 245 nm (Figs. S3 and S4 in Supporting information), which reached maximum after 2 equiv. of CB[8] was added, further supporting the 2:1 binging pattern. Adding CB[8] to the solution of **T1** (20 μmol/L) caused important hypochromic effect for the absorbance of **T1** around 245 nm. With the addition of about 20 μmol/L of **T1**, the hypochromic effect gave rise to an inflection point (Fig. S5 in Supporting information). By assuming that 97 % of 1:2 complex was formed, this result afforded a binding constant of $2.3 \times 10^{13}\ M^{-2}$ of low limit.

Dynamic light scattering (DLS) experiments were then performed for both **imSOF-1** and **imSOF-2** to study their concentration-dependent size changes (Fig. 2a and Fig. S6 in Supporting information). It was found that at the concentration of 30 and 15 μmol/L, the two frameworks displayed a hydrodynamic diameter (D_H) of 30 and 27 nm. Such sizes were expected to enable enhanced cell uptake through the endocytosis mechanism [59,60]. DLS indicated that **imSOF-1** was also stable in 1640 medium (Fig. S7 in Supporting information). Through the concentrations studied, the D_H values were also time-independent, which further confirmed the achievement of quick assembly and disassembly equilibrium of the frameworks at room temperature. ^{1}H NMR experiments in acetate-d_3-buffered D_2O (50 mmol/L, pH 4.74) showed that adding 0.28 mmol/L of *N*,*N*,*N*-trimethyl amantadine iodide (TMAM) (Fig. 1c), with which CB[8] forms 1:1 complex with high binding constant of $>10^{12}$ L/mol [61], to the solution of **imSOF-1** and **imSOF-2** ([**T1**] = 0.14 mmol/L, [**T2**] = 0.25 mmol/L,) caused complete substitution of **T1** or **T2** due to the formation of more stable 1:1 complex of TMAM with CB[8] (Fig S8 and S9 in Supporting information). As a result, compounds **T1** and **T2** displayed a set of high-resolution signals which was similar to that of the pure samples, while TMAM gave rise to another set of low-resolution signals comparable with those of the 1:1 complex of **T1** or **T2** with CB[8]. Accordingly, DLS profiles revealed the disappearance of the large nano-scaled frameworks. These observations solidly supported the dynamic and reversibility feature of the assembly and disassembly of the two SOFs at room temperature. Previously reported 4-phenylpyridinium-based SOFs do not undergo quick dissembling at room temperature [45]. Probably due to the deviation of the two N–C bonds of the imidazolium units from 180°, the 1,4-bis(imidazoliun)benzene units

of the tetrahedral precursors displayed higher conformational flexibility, which was expected to reduce the energy barrier for the decomposition of the SOFs at room temperature. As a result, the frameworks could undergo reversible concentration-dependent assembly and disassembly and be destroyed by TMAM to afford more stable binary complex with CB[8].

By using the diamond topology reported for 3D SOFs formed by 4-phenylpyridinium-based tetrahedral precursors, we could obtain an ideal 3D network for **imSOF-1** (Fig. 1a) [45]. Synchrotron small-angle X-ray scattering (SAXS) experiments were then conducted for **imSOF-1** in both the solid state and aqueous solution. The solid sample was obtained as powder by volatilizing the aqueous solution at room temperature and further drying the resulting solie *in vacuo*. The SAXS profile exhibited a peak with D-spacing of 1.6 nm, which should correspond to the (400) spacing (1.6 nm) of the modelled 3D network, supporting its periodicity in the solid phase (Fig. 2b). The solution of **imSOF-1** (**[T1]** = 0.2 mol/L) exhibited two wide, but clear peaks at the D-spacing of about 4.7 and 1.5 nm (Fig. 2c), which reasonably matched with the calculated (110) (4.8 nm) and (313) (1.5 nm) spacings, respectively, and supported that **imSOF-1** was also regular in solution. Considering that, for both **T1** and **T2**, CB[8] includes the peripheral aromatic units to form the 3D networks, it is reasonable to propose that **imSOF-2** gave rise to 3D networks with similar regularity. From the above diamondoid-styled 3D model, we could calculate that the pore defined by six neighboring CB[8] units in one self-assembled macrocycle, which adopted a cyclohexane-like chair conformation, had a size of 3.7 nm, which was substantially larger than that (2.1 nm) formed by 4-phenylpyridinium-derived tetrahedral components [45].

The biocompatibility of **imSOF1** and **imSOF2** were then assessed. Hemolysis experiments with human and rat red blood cells stored showed that, at the high concentration of 65.5 mg/mL, both SOFs did not cause important cell lysis (<3 %) (Fig. 2d and Fig. S10 in Supporting information). This safety dose was much higher than the highest dose (0.76 mg/kg) observed for reported 4-phenylpyridinium-based SOFs for cell lysis of <3 % [49]. With ICR mice model, the maximum tolerated dose (MTD) of the two SOFs was determined to be 120 and 105 mg/kg (Tables S1 and S2 in Supporting information), respectively. The value of **imSOF-1** was conspicuously higher than that (≤85 mg/kg) achieved by reported SOFs with ICR mice [49,52]. The body weights of the mice treated with **imSOF-1** of MTD were also recorded for 14 days (Fig. 2e). The body weights lost slightly during day 1, but recovered to grow as observed for the control group. The mice were euthanized on day 14 for organs (heart, liver, spleen, lungs and kidneys) harvesting and histopathological analysis of the tissue section. H&E results indicated no apparent differences between the mice treated with **imSOF-1** or **imSOF-2** and the mice treated with saline (Fig. 2f), indicating that both SOFs did not cause obvious damage to the main organs or cause light damage, from which the mice could recover quickly. Considering that **imSOF-1** had lower supramolecular weight and higher MTD and it was also easier to prepare **T1** than **T2**, we chose to use **imSOF-1** for further biofunctional studies.

The ability of **imSOF-1** for *in situ* adsorption and retention of antitumor drug doxorubicin (DOX) (Fig. 1d) was first evaluated using dialysis experiments (Fig. 2g). In a typical procedure [45], a solution of DOX (0.1 mmol/L) and **imSOF-1** (0.1 mmol/L) in phosphate-buffered saline (PBS) (1.5 mL, 50 mmol/L, pH 7.4) or acetate buffer (1.5 mL, 100 mmol/L, pH 4.5) in a dialysis bag (cut Mn: 1000 Da) was soaked in 15 mL of water in a test tube. The tube was shocked at 37 °C on a shaking table and the amount of DOX leaking to the outside solution was quantified by recording its UV–vis absorption spectra. It was found that at the physiological pH of 7.4, after 2 and 8 h, **imSOF-1** could retain 64 % and 51 % of DOX, while at acidic pH of 4.5, 75 % and 89 % of DOX diffused into the outside solution. Given the weakly acidic microenvironment of many tumors, these outcomes imply that, if the delivery of antitumor drugs by **imSOF-1** is realized, the acidic microenvironment of tumors may allow for controllable release of included drugs to gain efficacy enhancement. At both pH values, the leaking of DOX to the outside of the dialysis bag slowed down and reached the maximum after 8 h, which may be rationalized by considering that the concentration of DOX adsorbed in the framework decreased to the limit, at which the framework could maintain the adsorbed DOX molecules from further diffusing into the solution and to the outside of the bag.

Given that **imSOF-1** had MTD of 120 mg/kg, we designed the following *in vivo* test for DOX delivery and antitumor efficacy assessment for female nude BALB/c mice (5 weeks) implanted with multidrug-resistant MDR A549/ADR tumor on the back. Twenty mice were randomly divided into 4 groups: Group 1 treated with PBS, Group 2 treated with **imSOF-1**, Group 3 treated with DOX, and Group 4 treated with DOX and **imSOF1–1**. On day 0, 3, 6, and 10, the mice were injected intravenously with 0.2 mL of PBS, **imSOF-1** (20 mg/kg), DOX (4 mg/kg), and **imSOF-1** (20 mg/kg) and DOX (4 mg/kg), respectively, for totally 4 times. All the mice were monitored for 12 days and their body weight was recorded every day (Fig. 3a). It was found that there was no significant difference of the body weight of Groups 1 and 2, indicating that **imSOF-1** had no additional toxicity. The first injection caused the body weight of Group 4 decreased by about 5 %, but during the following days with another three times of injections, the body weight of this group was generally stable, and throughout the 12 days of observation, all the mice did not show weary symptoms. The tumor volume was measured and calculated using equation of $V = L \times W^2/2$, where L and W represent the length and width, respectively (Fig. 3b). On day 12 all the mice were euthanized for harvesting the tumors and main organs (Fig. 3c). It was found that, compared with Groups 1 and 2, Group 3 did not show observable efficacy of DOX for the first two injections. The last two injections of DOX slightly slowed down the growth of the tumors and, compared with that of Group 1, the weight of the tumors on day 12 was estimated to reduce by 13 %. For Group 4, the weight reduced by 66 %, which indicated that the delivery of **imSOF-1** caused 5.1-fold enhancement of the efficacy of DOX (Fig. 3d). From each group, one mouse was chosen randomly for collecting its main internal organs (heart, liver, brand, lung, kidney), and H&E-stained sections were made, which revealed no significant damage for Groups 2 and 4. These results supported that **imSOF-1** displayed important delivery ability, but did not cause toxicity (Fig. S11 in Supporting information). The pathology of the tumor tissues harvested from euthanized mice on day 12 was also investigated using Ki-67, TUNEL and H&E staining (Fig. 3e). Ki-67 staining showed that group 4 displayed the lowest expression of antigen Ki-67 and thus supported that DOX in the presence of **imSOF-1** exhibited the highest efficacy in suppressing tumor growth. TUNEL staining also showed that **imSOF-1** remarkably enhanced the ability of DOX to induce the apoptosis of the tumor cells, while H&E staining revealed more severe necrosis of the tumor of Group 4 relative to Group 3. All the results supported that **imSOF-1** enhanced the antitumor activity of DOX.

Photofrin (PTF) is the most widely used photodynamic agent, but suffers serious phototreatment shin phototoxicity, which lasts up to two months, during which patients have to avoid exposure to sunlight or room light after treatment [62]. Previous investigations show that 4-phenylpyridinium or *N*-phenylimidazonium-derived SOFs can adsorb PTF through hydrophobic and ion-pair electrostatic attraction [50,52]. Photofrin aggregates into large nanoparticles in water and thus the adsorption of SOFs for it could not be investigated using dialysis experiment [50]. Adding **imSOF-1** to its solution in water caused important hypochromic effect and

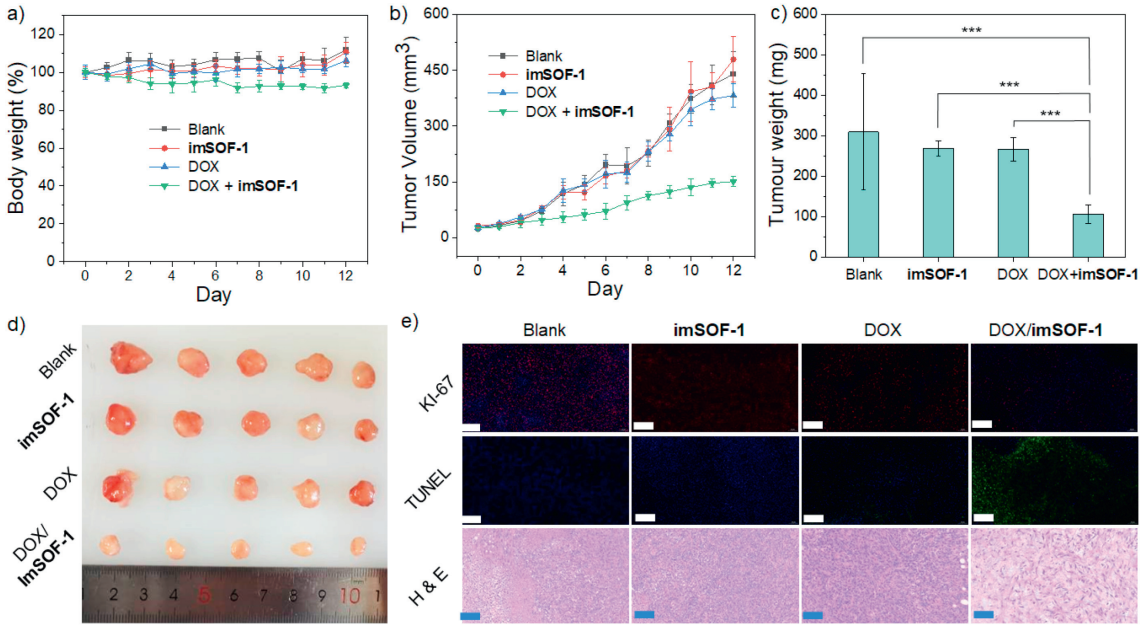


Fig. 3. (a) Body weight of MDR A549/ADR tumor-implanted mice after treated with saline, **imSOF-1**, DOX and DOX/**imSOF-1**. (b) Tumor volume *versus* the day monitored. (c) Average excised tumor weight of each group. (d) Photographs of tumor tissues obtained on day 12 after the 1st administration ($n = 5$). (e) Micrographs of Ki-67, TUNEL and H&E-stained tumor tissues collected from each group (scale bar: 200 μm).

bathochromic shifting (Fig. S12 in Supporting information), which evidenced that the framework included the photosensitizer to affect its absorbance.

Given the unprecedentedly high MTD of **imSOF-1**, we further evaluate its ability for inhibiting the posttreatment phototoxicity of PTF, using BALB/c nude mice bearing B16-F10 melanoma tumors as animal models. Sixteen B16-F10 melanoma tumor-inoculated BALB/c nude mice (female, 5 weeks) were randomly divided into four groups ($n = 4$): Group 1 treated with saline (0.2 mL), Group 2 treated with PTF (4 mg/kg, 0.2 mL), Group 3 treated with (PTF (4 mg/kg) and **imSOF-1** (10 mg/kg), 0.2 mL), and Group 4 treated with (PTF (4 mg/kg) and **imSOF-1** (20 mg/kg), 0.2 mL). All the treatments were conducted through intravenous injection of the tail. After standing in the dark for 24 h, the tumor section of the mice was irradiated with a laser at a wavelength of 635 nm (100 mW/cm^2) for 7 min and the mice were left to stand for another 4 h in the dark. Then their dorsal skin was irradiated with a solar simulator (100 mW/cm^2) for 30 min, and then the mice were left in the dark for body weight and tumor volume monitoring for 10 days. On the last day, the mice were euthanized to collect the tumor tissues for further activity and biosafety assessments. All mice showed normal body growth, even though Group 1 lost body weight slightly (Fig. 4a), which may be attributed to the tumor growth-led deterioration. Regarding the antitumor activity (Fig. 4b), the tumor growth of Groups 2 and 3 was comparable, but for Group 4, the growth was discernibly quicker. These results indicated that the dose of 10 mg/kg of **imSOF-1** did not lead to important suppression for the efficacy of PTF, while the dose of 20 mg/kg did. A comparison of the tumor volume and weight collected for the mice finally euthanized is also consistent with the above observation (Fig. 4c). Exposing to the irradiation of simulated sunlight did not cause mice of Groups 1, 3 and 4 to suffer observable skin damage (Fig. 4d and Fig. S13 in Supporting information). In contrast, mice of Group 2 treated with PTF showed serious skin damage on day 2, which deteriorated on day 4. Although the damaged skin then gradually scabbed, but did not recover even on day 10. These results clearly supported that **imSOF-1** could suppress the post-treatment phototoxicity of PTF and is more efficient than two reported SOF systems [50,52], which alleviate, but do not eliminate the posttreatment phototoxicity of PTF.

Finally, we further assessed the ability of **imSOF-1** in neutralizing the anticoagulating activity of unfractionated heparin (UFH) and low molecular weight heparins (LMWHs), including dalteparin (Dalte), enoxaparin (Enox) and nadroparin (Nadro). Both heparins are clinically applied to prevent and treat venous thromboembolism and atherothrombotic syndromes, but suffer from incidence of hemorrhagic complications and lack a safe and universal antagonist [63]. The assessment was conducted with bovine plasma by testing the activated partial thromboplastin time (aPTT) in the presence of the heparins of the identical dose of 2.0 IU/mL. For comparison, incremental doses of **imSOF-1** and protamine (PTA), the clinically used antagonist for UFH, were added and their efficacy for neutralizing the activity of the four heparins are obtained (Figs. 5a-d). It was found that, for UFH, **imSOF-1** could achieve 100 % neutralization of its anticoagulating activity with the dose from 0.03 mg/kg to 0.07 mg/kg. For Enox, Nadro and Dalte, **imSOF-1** at the dose of 0.072, 0.075, and 0.07 mg/kg could accomplish nearly 100 % neutralization, while within the dose range of 0.04–0.08, 0.055–0.085, and 0.025–0.085 mg/kg, 90 % neutralization could be realized. For all the four heparins, PTA showed a notably lowered neutralization ability and also a much narrower concentration window, which is consistent with its clinical performance. That is, it can completely neutralize the activity of UFH, but for the three LMWHs, can gain only ≤70 % of neutralization [64,65]. Although **imSOF-1** of high dose also displayed anticoagulating activity, which is common for all reported heparin antidotes, it possessed a much wider concentration window than PTA for all the heparins. Thromboelastographic (TEG) assessment was further conducted with human whole blood (HWB) to evaluate the validation of **imSOF-1** to neutralize heparins under an approximately physiological condition. For this assessment, HWB samples (1.0 mL) were anticoagulated with different heparins (2.0 IU/mL) and then treated with **imSOF-1** of varying concentrations to observe the clotting characteristics of the samples (Figs. 5e and f, Figs. S14 and S15 in Supporting information). It was found that with, at the dose ranges of 15–40, 15–45, 20–30 and 30–45 μg/mL, **imSOF-1** could

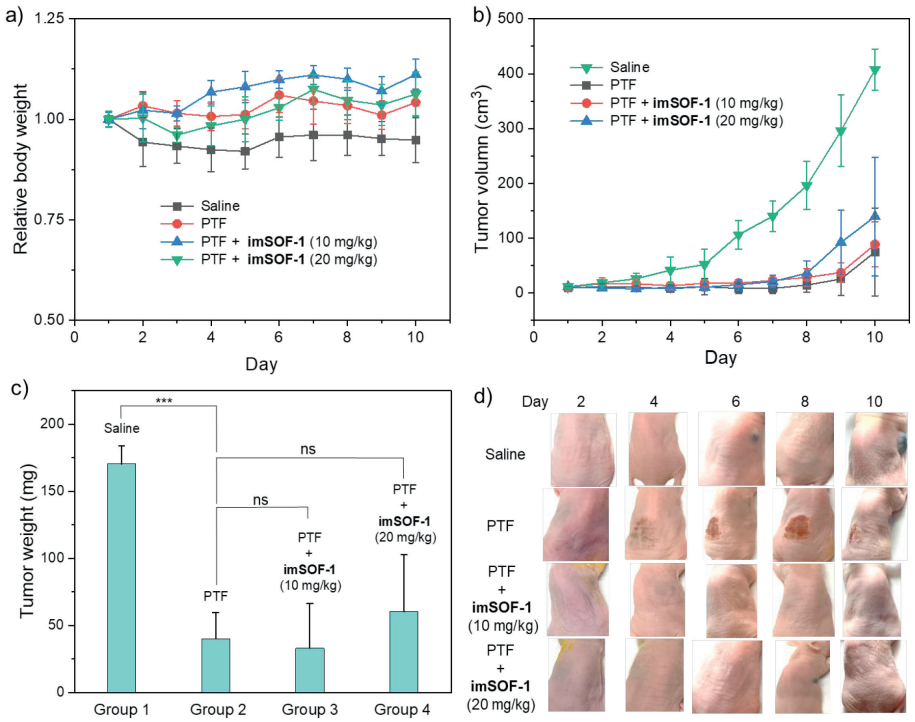


Fig. 4. The effect of **imSOF-1** on the photodynamic therapeutic activity and posttreatment phototoxicity of PTF *in vivo*. (a) Body weight of mice *versus* the day monitored. (b) Volume of tumors *versus* the day monitored. (c) Body weight of tumors harvested on the last day. (d) Images of the same mouse taken on different days after administration.

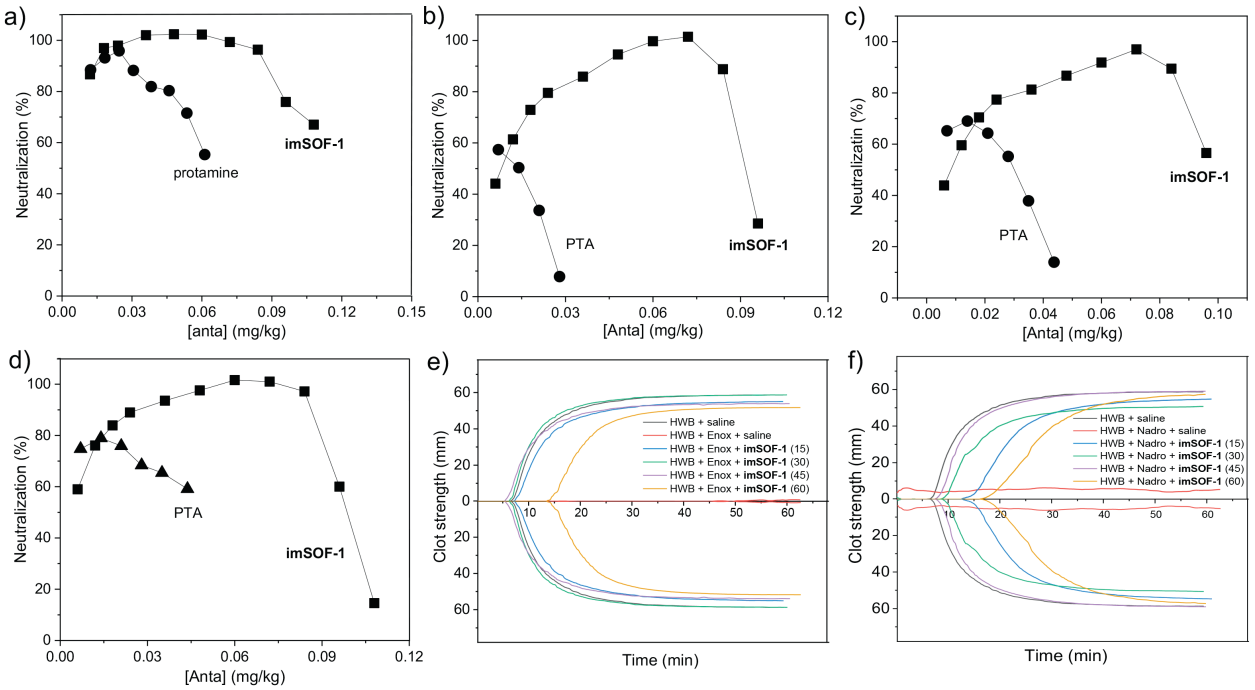


Fig. 5. (a-d) APTT assays in bovine plasma for the neutralization of UFH, Enoxa, Nadro and Dalte (2.0 IU/mL) by incremental dose of **imSOF-1** and PTA. (e, f) TEG assays for neutralization of Enoxa and Nadro (2.0 IU/mL) by **imSO-F1** in HWB.

cause the clot strength of HWB to recover to the normal one observed for normal HWB treated with saline.

In summary, we have constructed two new SOFs through co-assembly of imidazolium-derived tetrahedral components and CB[8], which features reversible assembly and disassembly at room temperature and the highest maximum tolerated dose. One of the new SOFs (**imSOF-1**) is revealed to function well as porous carrier for doxorubicin inclusion and intracellular delivery to achieve enhance antitumor efficacy by overcoming multidrug resistance of the tumor. The new SOF can also include photofrin to inhibit its posttreatment phototoxicity and various heparins to neutralize their anticoagulation activity. For the delivery of doxorubicin of 4 mg/kg dose, 20 mg of **imSOF-1** is used for achieving notably enhanced antitumor efficacy. Given its MTD of 120 mg/kg with mice, this dose holds promise for further preclinical evaluation. However, further improvement of biosafety will increase the promise. One

possible approach for this aim is to modify the surface of SOFs using polyethylene glycols, which may endow SOFs with stealth characteristics of increased biosafety and long circulation. By maintaining the assembly reversibility at room temperature, such SOFs should possess increased promise for preclinical investigations.

Ethical statement

Animal experiments were performed in agreement with the guidelines of the Animal Care and Use Committee of Fudan University (2024-CHEM-026). Scientific research with human whole blood, which was provided by the Shanghai Blood Center, was approved by the Shanghai Municipal Commission of Health and Family Planning (HXB-2024–15).

Declaration of competing interest

The authors declare that they have no known competing financial interests or personal relationships that could have appeared to influence the work reported in this paper.

CRediT authorship contribution statement

Ya-Jie Zhu: Writing – original draft, Investigation. **Zhi-Min Lv:** Conceptualization. **Hao-Feng Zhu:** Investigation. **Qi-Yan Qi:** Investigation. **Shang-Bo Yu:** Methodology, Conceptualization. **Jia Tian:** Supervision, Resources, Formal analysis. **Wei Zhou:** Supervision, Methodology, Data curation, Conceptualization. **Zhan-Ting Li:** Writing – review & editing, Supervision, Resources, Funding acquisition, Data curation, Conceptualization.

Acknowledgments

We thank the National Natural Science Foundation of China (No. 21921003 for Z.T.L. and 22201293 for S.B.Y.) and Shanghai Sailing Program (No. 22YF1458300 for S.B.Y.) for financial support. We are grateful to Shanghai Synchrotron Radiation Facility of BL16B1 for the assistance on SAXS measurements.

Supplementary materials

Supplementary material associated with this article can be found, in the online version, at doi:10.1016/j.cclet.2025.111353.

References

[1] M. Fialkowski, K.J.M. Bishop, R. Klajn, et al., J. Phys. Chem. B 110 (2006) 2482–2496.
[2] X.Y. Hu, T. Xiao, C. Lin, F. Huang, L. Wang, Acc. Chem. Res. 47 (2014) 2041–2051.
[3] S. Roy, P.P. Pillai, Langmuir 39 (2023) 12967–12974.
[4] S. Mura, J. Nicolas, P. Couvreur, Nat. Mater. 12 (2013) 991–1003.
[5] X. Wu, L. Gao, X.Y. Hu, L. Wang, Chem. Record. 16 (2016) 1216–1227.
[6] W. Feng, M. Jin, K. Yang, Y. Pei, Z. Pei, Chem. Commun. 54 (2018) 13626–13640.
[7] P. Li, Y. Chen, Y. Liu, Chin. Chem. Lett. 30 (2019) 1190–1197.
[8] Z. Zheng, W.C. Geng, Z. Xu, D.S. Guo, Isr. J. Chem. 59 (2019) 913–927.
[9] N. Song, Z. Zhang, P. Liu, et al., Adv. Mater. 32 (2020) 2004208.
[10] P. Zhang, M. Li, C. Xiao, X. Chen, Chem. Commun. 57 (2021) 9489–9503.
[11] Z. Wang, C. Sun, R. Wang, Bioconjug. Chem. 33 (2022) 2254–2261.
[12] X. Li, M. Shen, J. Yang, L. Liu, Y.W. Yang, Adv. Mater. 36 (2024) 2313317.
[13] Y.Y. Liu, X.Y. Yu, Y.C. Pan, et al., Sci. China Chem. 67 (2024) 1397–1441.
[14] Y. Liu, Y. Wu, Z. Luo, M. Li, iScience 26 (2023) 106279.
[15] M. Hou, S. Liu, Biomacromolecules 25 (2024) 5402–5416.
[16] Y. Zhao, Q. Huang, Y. Liu, ChemBioChem 25 (2024) e202400635.
[17] W. Yan, T. Lang, R. Zhu, et al., Nano Today 42 (2022) 101376.
[18] Y. Chen, Z. Huang, H. Zhao, et al., ACS Appl. Mater. Interfaces 9 (2017) 8602–8608.
[19] Y.F. Ding, J. Wei, S. Li, et al., ACS Appl. Mater. Interfaces 11 (2019) 28665–28670.
[20] M.P. Li, N. Yang, W.R. Xu, Beilstein J. Org. Chem. 18 (2022) 539–548.
[21] Y. Yin, P. Zeng, Y. Duan, et al., J. Mater. Chem. B 12 (2024) 8099–8106.
[22] M. Kapoor, S.L. Lee, K.M. Tyner, AAPS J. 19 (2017) 632–641.
[23] S.S. Godase, N.S. Kulkarni, S.N. Dhole, Adv. Pharm. Bull. 14 (2024) 34–47.
[24] G. Murphy, D.J. Brayden, D.L. Cheung, et al., J. Control. Release 380 (2025) 375–395.
[25] E. Bernabeu, M. Cagel, E. Lagomarsino, M. Moretton, D.A. Chiappetta, Int. J. Pharm. 526 (2017) 474–495.
[26] B.S. Pattni, V.V. Chupin, V.P. Torchilin, Chem. Rev. 115 (2015) 10938–10966.
[27] S. Walker, R. Oun, F.J. McInnes, N.J. Wheate, Isr. J. Chem. 51 (2011) 616–624.
[28] L. Isaacs, Acc. Chem. Res. 47 (2014) 2052–2062.
[29] D. Shetty, J.K. Khedkar, K.M. Park, K. Kim, Chem. Soc. Rev. 44 (2015) 8747–8761.
[30] S.J. Barrow, S. Kasera, M.J. Rowland, J. del Barrio, O.A. Scherman, Chem. Rev. 115 (2015) 12320–12406.
[31] H. Yin, Q. Cheng, D. Bardelang, R. Wang, JACS Au 3 (2023) 2356–2377.
[32] J.H. Hu, Y. Huang, C. Redshaw, Z. Tao, X. Xiao, Coord. Chem. Rev. 489 (2023) 215194.
[33] O.A.A. Alabrahim, S.A. Fahmy, H.M.E.S. Azzazy, ACS Appl. Nano Mater. 6 (2023) 3139–3158.
[34] S. Shukla, B. Sagar, A.K. Sood, et al., ACS Appl. Bio Mater. 6 (2023) 2089–2101.
[35] S.B. Yu, W. Zhou, J. Tian, et al., Sci. Sinica Chim. 53 (2023) 2345–2356.
[36] L. Armstrong, S.L. Chang, N. Clements, et al., Chem. Soc. Rev. 53 (2024) 11519–11556.
[37] L. Mao, S. Li, X. Zhang, Z.T. Li, D. Ma, Chin. Chem. Lett. 35 (2024) 109363.
[38] J. Li, Y. Zhang, S. Liu, Chin. Chem. Lett. 35 (2024) 109645.
[39] Z. Dai, L. Tan, Y. Su, et al., Chin. Chem. Lett. 35 (2024) 109121.
[40] Y.H. Ko, E. Kim, I. Hwang, K. Kim, Chem. Commun. (2007) 1305–1315.
[41] Y. Liu, H. Yang, Z. Wang, X. Zhang, Chem. Asian J. 8 (2013) 1626–1632.
[42] Y. Lu, Z. Yu, X. Yang, et al., Chin. Chem. Lett. 34 (2023) 108040.
[43] H. Nie, D. Hu, Z. Zeng, et al., Sci. China Chem. 67 (2024) 1605–1612.
[44] C. Wang, L. Xu, Z. Jia, T.P. Loh, Chin. Chem. Lett. 35 (2024) 109075.
[45] J. Tian, T.Y. Zhou, S.C. Zhang, et al., Nat. Commun. 5 (2014) 5574.
[46] J. Tian, C. Yao, W.L. Yang, et al., Chin. Chem. Lett. 28 (2017) 798–806.
[47] C. Yao, J. Tian, H. Wang, et al., Chin. Chem. Lett. 28 (2017) 893–899.
[48] B. Yang, X.D. Zhang, J. Li, et al., CCS Chem. 1 (2019) 156–165.
[49] F. Lin, S.B. Yu, Y.Y. Liu, et al., Adv. Mater. 34 (2022) 2200549.
[50] Y. Liu, C.Z. Liu, Z.K. Wang, et al., Biomaterials 284 (2022) 121467.
[51] Z.T. Li, S.B. Yu, Y. Liu, J. Tian, D.W. Zhang, Acc. Chem. Res. 55 (2022) 2316–2325.
[52] L. Zhang, Y.Y. Liu, Y. Zong, et al., ACS Appl. BioMater. 8 (2025) 792–802.
[53] K. Gajera, A. Patel, J. Adv. Med. Pharm. Sci. 24 (2022) 1–7.
[54] M. Sameer Khan, G. Gupta, A. Alsayari, et al., Int. J. Pharm. 658 (2024) 124212.
[55] S.Y. Jon, Y.H. Ko, S.H. Park, et al., Chem. Commun. (2001) 1938–1939.
[56] D.J. Tranchemontagne, Z. Ni, M. O'Keeffe, O.M. Yaghi, Angew. Chem. Int. Ed. 47 (2008) 5136–5147.
[57] S.M. Walter, F. Kniep, E. Herdtweck, S.M. Huber, Angew. Chem. Int. Ed. 50 (2011) 7187–7191.
[58] J. Tian, Y.D. Ding, T.Y. Zhou, et al., Chem. Eur. J. 20 (2014) 575–584.
[59] J. Dolai, K. Mandal, N.R. Jana, ACS Appl. Nano Mater. 4 (2021) 6471–6496.
[60] D. Ma, J. Zhang, Y.Y. Liu, et al., Sci. China Chem 68 (2025) 3660–3666.
[61] S. Liu, C. Ruspic, P. Mukhopadhyay, et al., J. Am. Chem. Soc. 127 (2005) 15959–15967.
[62] M.C. Tougherty, T. Mang, Lasers Surg. Med. 10 (1990) 485–488.
[63] B. Ourri, L. Vial, ACS Chem. Biol. 14 (2019) 2512–2526.
[64] Y. Zong, Z. Lei, S.B. Yu, et al., J. Med. Chem. 67 (2024) 3860–3873.
[65] M. Crowther, T. Warkentin, Blood 111 (2008) 4871–4879.